Journal of Asian Earth Sciences 169 (2019) 199–209

Contents lists available at ScienceDirect

Journal of Asian Earth Sciences

journal homepage: www.elsevier.com/locate/jseaes

Full length article

Qualitative appraisal of high resolution satellite derived free air gravity anomalies over the Maldive Ridge and adjoining ocean basins, western Indian Ocean

Priyesh Kunnummal, S.P. Anand*

Indian Institute of Geomagnetism, Navi Mumbai, Maharashtra 410218, India

A R T I C L E I N F O

Keywords:
Maldive Ridge
Free air gravity anomaly
Wavelength filtering
Power spectrum
Magmatic underplating

A B S T R A C T

High resolution satellite derived Free Air Gravity (FAG) anomalies over the Maldive Ridge segment of the Chagos-Laccadive Ridge and adjoining areas of the Arabian Basin and Central Indian Basin was analyzed to understand their structure. Indian Ocean Geoidal Low corrected FAG depict the N-S trending relative highs associated with the Maldive Ridge, the lows associated with the Vishnu Fracture Zone, and the seafloor fabrics associated with spreading Central Indian Ridge in the Arabian Basin. Transformation operations for enhancing the short, intermediate and long wavelength anomalies were carried out. The northward continuation of the Vishnu Fracture Zone, the eastward extension of the fracture zones of the Arabian Basin into the Deep Sea Channel (DSC) region, between the Maldive Ridge and the Chagos Bank, and the signatures related to north-south trending coral reefs have been deciphered from the enhancement of short wavelength anomalies. The long wavelength anomalies show N-S highs along the axis of the Maldive Ridge and the DSC, which on comparison with previous studies, is inferred to be the signature related with the underplated material from the passage of the Indian plate over the Reunion Plume. Depth to top of two interfaces over the Maldive Ridge and the DSC were computed using the power spectral method by assuming a window of 110 km dimension and 50 km overlap. Depths were thus calculated for 44 blocks along the ridge axis. The average depth to the top of the shallow interface was found to be 5.5 km while that of the deeper was 11.0 km. These depths and interfaces were confirmed by undertaking 2D forward modelling along a 300 km long N-S profile along the western segment of the Maldive Ridge. Integrating with the available previous geophysical studies, it is inferred that the shallow interface represents the depth to the top of the acoustic basement underlying 1–1.5 km thick lava flow unit while the deeper is associated with the interface between the crust and initial Moho before the underplating took place (presently top of the underplated material). From the present study, it has been inferred that the Deep Sea Channel between the Maldive Ridge and Chagos Bank can be purely oceanic in nature.

1. Introduction

The Chagos-Laccadive Ridge (CLR) is a N-S trending aseismic feature stretched over 3000 km along the meridional direction between 15°N and 10°S (Fig. 1). The ridge is divided into three main segments: the northern segment referred to as Laccadive Plateau, the middle Maldive Ridge and the southern Chagos Bank (Bhattacharya and Chaubey, 2001). An archipelago of coral islands rest on each of the segments with the ridge crest comprising of shoals, banks and corals reefs at depths less than 1500 m. The Maldive Ridge segment of the CLR lies approximately between 7°N and 1°S (Bhattacharya and Chaubey, 2001). The islands of Chagos, the Maldives and Lakshadweep are above-water parts of the Chagos-Laccadive Ridge. The Lakshadweep-Maldives-Chagos Archipelago comprises the most extensive coral reef and atoll community in the Indian Ocean as well as the largest atoll system in the world. Several hypotheses were put forth regarding the genesis of CLR (Bhattacharya and Chaubey, 2001 and references therein): a zone of transition between oceanic crust in the west and continental crust in the east, a leaky transform fault, a hot spot trace, or a micro-continent. Different segments of the CLR having different genesis has also been postulated (Bhattacharya and Chaubey, 2001 and references therein), for example, Chagos Bank may be composed of volcanic material associated with leaky transform fault, the Maldives as a microcontinent, Laccadive Plateau as a continental fragment etc. Recently, from the recovery and dating of zircons (Ashwal et al., 2017) from the basaltic beach sands of Mauritius, the existence of an ancient

* Corresponding author.
E-mail address: aerospl@yahoo.co.uk (S.P. Anand).

https://doi.org/10.1016/j.jseaes.2018.08.008
Received 9 December 2017; Received in revised form 8 July 2018; Accepted 10 August 2018
Available online 13 August 2018

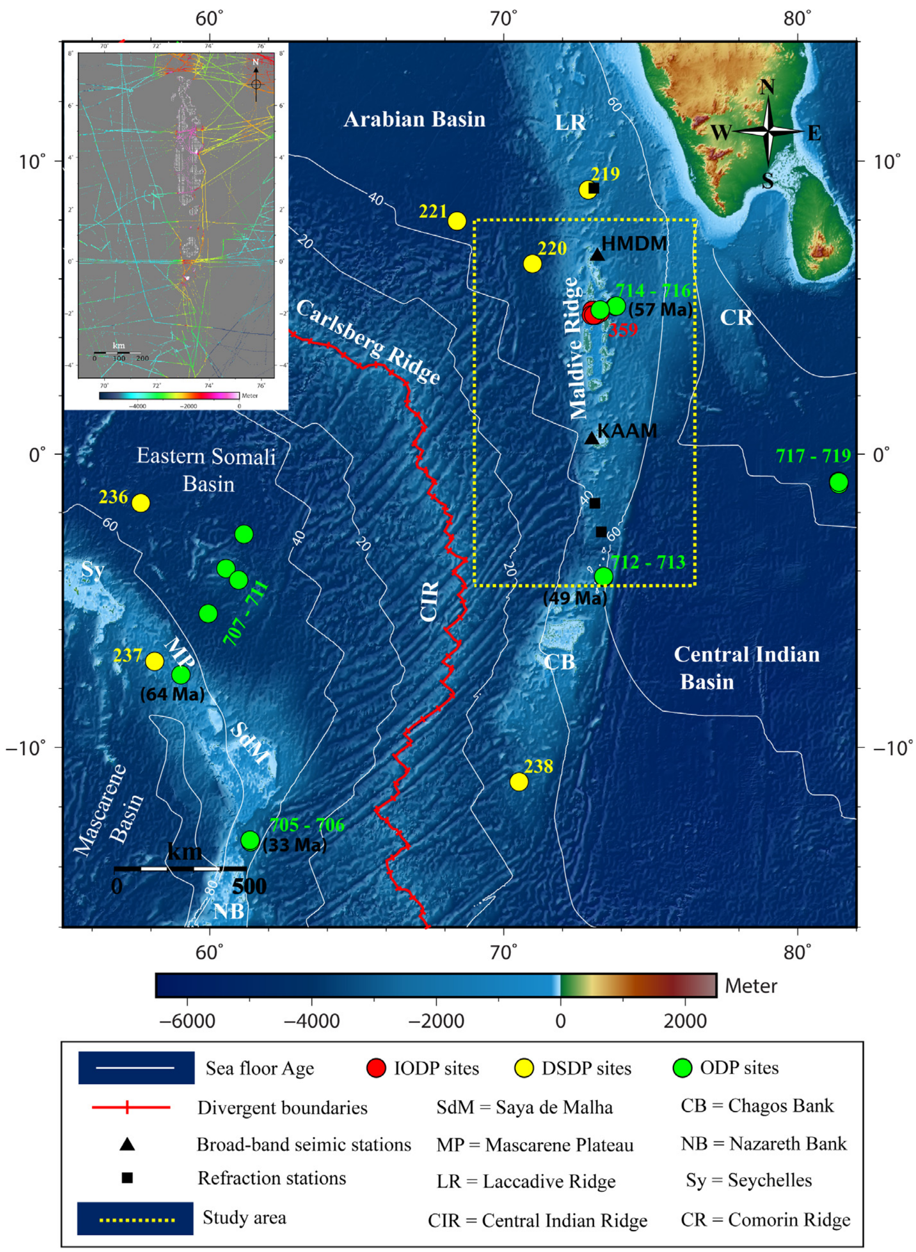

Fig. 1. Bathymetry map of the Western Indian Ocean generated from satellite altimetry (Smith and Sandwell, 1997) depicting major structural and tectonic features in the study region and adjoining areas. Dotted rectangle demarcates the region under study. White solid lines represent contoured magnetic isochrones (Müller et al., 2008). The solid black triangles and boxes respectively indicate broadband seismic stations (Fontaine et al., 2015) and seismic refraction stations (Francis and Shor, 1966). Locations of ODP well site (Backman et al., 1988) represented by solid green circles and IODP by red circles (Betzler et al., 2017). Value in bracket is the age of the volcanic flows. **CIR**: Central Indian Ridge, **LR**: Laccadive Ridge, **CB**: Chagos Bank, **Sy**: Seychelles, **SdM**: Saya de Malha, **MP**: Mascarene Plateau, **NB**: Nazareth Bank. **CR**: Comorin Ridge. Inset shows density of depth soundings data utilized for the generation of bathymetry in the study region. (For interpretation of the references to colour in this figure legend, the reader is referred to the web version of this article.)

continental crust beneath Mauritius was hypothesized. Mauritius, Saya de Malha, Chagos, Cargados-Carajos Banks, Laccadives and Nazareth were postulated to be part of this Precambrian micro-continent coined “Mauritia” (Torsvik et al., 2013). Through the crustal thickness mapping of Mauritius and adjoining regions using inversion of gravity data, Torsvik et al. (2013) argued that Mauritius formed part of a contiguous block of anomalously thick crust (> 25–30 km) that extends in an arc northwards to the Seychelles. Previous geophysical studies conducted over the Laccadive Ridge segment of the CLR have suggested the ridge to be of continental origin (Ajay et al., 2010; Chaubey et al., 2008) and that the ridge was a part of the Western Dharwar craton bounded by the Chapporo lineament to the north and Bhavani shear to the south (Nair et al., 2013). Compared to the number of geophysical studies undertaken to understand the structure of most of the aseismic ridges in the Indian Ocean, the Maldive-Chagos part of the Chagos-Laccadive Ridge is least studied. Few industrial wells were drilled over the Maldive Ridge segment (Aubert and Droxler, 1996) of the CLR in addition to the few wells drilled under ODP and IODP programs (Duncan and Hargraves, 1990; Betzler et al., 2017). Other geophysical studies include few industrial seismic reflection surveys in the Maldive Inner Sea area (Aubert and Droxler, 1996), receiver function analysis from broadband seismic stations (Fontaine et al., 2015) located at Huvadhu atoll and Haa Dhaalu atoll, respectively in the southern and northern part of the Maldive Ridge (Fig. 1). To better understand the structures related to the Maldive Ridge it is essential to look at a data set which has uniform coverage, such as satellite altimetry derived free-air gravity data. The availability of satellite derived geopotential data is very helpful in deciphering the structures where traditional ship borne geophysical data are either not available or sparse. The accuracy and resolution of the free-air gravity anomalies derived from satellite radar altimeter data have improved over the years, and these data are now of increasing value for modelling structures of interest in the oil industry as well as providing regional geological information (Majumdar et al., 1998). An evolutionary model of the Laccadive Ridge segment of the CLR was provided by Nair et al. (2013) from the analysis of satellite derived free-air anomalies and using different wavelength filtering techniques. In the present paper an attempt has been made to have qualitative appraisal of the High resolution satellite derived free-air gravity anomalies and its various transformations based on wavelengths and compare the results with the available geophysical data sets to improve our understanding of the structure of the Maldive Ridge segment and the Deep Sea Channel region of the Chagos-Laccadive Ridge.

2. Morpho-tectonic elements and previous studies

The major morpho-tectonic elements in the study region encompass the north-south trending Maldive Ridge, the Deep Sea Channel between the Maldive Ridge and Chagos Bank and the ocean floor of adjacent Arabian and Central Indian Basins (Fig. 1). The Maldive Ridge, which lies approximately between 7° N and 1° S, is bounded in the west by NE-SW trending seafloor fabrics of Arabian Basin and in the East by the Central Indian Basin. An archipelago of coral islands grouped in a double row of atolls separated by an inner sea rest on the Maldive Ridge. The volcanic basement of the Ridge is overlain by 3-km thick Eocene and Oligocene neritic carbonates (Belopolsky and Droxler, 2004). Eight IODP wells (expedition 359, Betzler et al., 2017) and three ODP wells (leg 115, sites 714,715,716, Backman et al., 1988) were drilled in the northern part of the Maldive Ridge (location shown in Fig. 1). Among this, the well 715 reached up to an olivine basaltic basement of Early Eocene (57 Ma) age, around 211 m below seafloor (Backman et al., 1988). Through the inversion of gravity data, Torsvik et al. (2013) suggested a crustal thickness ≥25–30 km beneath the Laccadives, Maldives and Chagos. The receiver function studies of Fontaine et al. (2015) also reported a broader crust-mantle transition and thicker crust over the Maldive Ridge with the Moho lying at ~23 km and an initial Moho, before the formation of magmatic underplated rocks, at ~13 km below the KAAM station (location shown in Fig. 1). The Deep Sea Channel area between the Maldive Ridge and Chagos Bank is about 4500 m deep; the seismic refraction studies (Francis and Shor, 1966) suggested that this region is underlain by a thick 1 km layer of 2.15 km/s velocity material at the top, below which lies about 4 to 5 km thick layer of velocity 6.13 km/s possibly representing volcanic material. According to the hotspot genesis model, this area interrupts the typically continuous hotspot track between the Maldives and the Chagos Bank and originated from a combination of the ridge geometry, in particular the distribution of transform faults, plate motions and plume-ridge interaction (Bredow et al., 2017). Well-defined sea-floor spreading anomalies related to young ocean floor were identified in the Arabian Basin to the west of MR while in the Central Indian Basin (McKenzie and Sclater, 1971) the oldest spreading anomalies identified was A34 (Cande and Patriat, 2015), related to the spreading of India and Madagascar. However, no spreading anomalies were identified along the Chagos-Laccadive Ridge (Avraham and Bunce, 1977).

3. Data source and methodology

In the present study, the most recent global marine free-air gravity model (Version 24.1, Sandwell and Smith, 2009; Sandwell et al., 2014) which comprises twelve more months of CryoSat-2 altimeter data in addition to the previous Version 23.1, has been utilized. These data are two times more accurate than all previous models with an accuracy of about 2mGal and ensures high clarity with more improvements at short wavelength band - 12–40 km (Sandwell et al., 2014). The bathymetric data used are the latest one arc minute resolution global seafloor topography (Version 18.1, Smith and Sandwell, 1997) derived by combining all of the available depth soundings with high-resolution marine gravity information from satellite altimetry. The density of depth soundings data utilized for the generation of bathymetry in the study region is shown as an inset in Fig. 1. Both the above gravity and bathymetric data sets are well suited for regional tectonic investigation studies since they contain required wavelength information, with uniform coverage and accuracy. The free-air gravity data over the study region are largely influenced by the gravity effect of Indian Ocean Geoidal low (IOGL) (Kahle et al., 1978) centred east of Comorin Ridge and south of Sri-Lanka. The IOGL spans over very large areal distance as a long wavelength feature with a significant low of −106 m in geoid height in the Indian Ocean, south of the Indian sub-continent (Sreejith et al., 2013). Using the spherical harmonic coefficient of EIGEN-6C4 Geoid model (Förste et al., 2015) up to degree and order 50 (the coefficients are gently rolled off between the degrees 30–70 in order to avoid the ringing effect arising due to sharp truncation at the degree 50), the gravity contribution of IOGL is calculated and removed from free-air gravity data. The geoid corrected free-air gravity anomaly (FAG-IOGL), which typically contains information up to upper mantle is used for qualitative evaluation and interpretation of major tectonic elements in the study region.

Various transformation operations and wavelength filtering have been carried out using the FAG-IOGL map, to enhance the shallow and deeper features along the Maldive Ridge (MR), Deep Sea Channel (DSC) and the adjoining ocean floor. To enhance the signature from the shallow features represented by high-frequency components we have utilized the first vertical derivative (Blakely, 1995) and analytic signal method (Nabighian, 1984) to map the source distribution at shallow levels. In addition, we have used Butterworth high pass and low pass filters to retain the short and long wavelength anomalies, respectively.

Radially averaged power spectrum was computed over MR and DSC to compute the depth to the top of interfaces with varying density contrast. Radially averaged power spectrum of gravity and magnetic data can be used to obtain average depth to the top of the density or magnetization interfaces at different depth levels (Spector and Grant, 1970; Mishra and Pedersen, 1982). In the Fourier domain, the equivalent layer theorem states that to first order the gravity spectrum at the surface due to a subsurface layer with relief spectrum $\Delta z(k)$, depth z_0 and density contrast $\Delta\rho$ in 2D is given by (Karner, 1982)

$$\Delta g(k) = 2\pi G \Delta\rho e^{-2\pi|k|z_0} \Delta z(k)$$

whose power spectrum can be expressed as

$$|\Delta g(k)|^2 = (4\pi^2 (\Delta\rho G)^2 e^{-4\pi|k|z_0}) |\Delta z(k)|^2$$

Taking the natural logarithm of the radially averaged power spectrum, the above equation becomes,

$$\ln\langle|\Delta g(k)|^2\rangle = -4\pi z_0 \; |k| + \ln[4\pi^2(\Delta\rho G)^2 \langle|\Delta z(k)|^2\rangle]$$

where $\langle\rangle$ denotes the radial average (Spector and Grant, 1970). Assuming, random uncorrelated sources $\langle|\Delta z(k)|^2\rangle$ becomes one and ln $(4\pi^2(\Delta\rho G)^2)$ becomes constant. The above equation can then be approximated as a straight line of slope $-4\pi z_0$ in which z_0 may be found by plotting the natural logarithm of the radially-averaged power spectrum against the wavenumber, $|k|$ (Blakely, 1995). In reality, the sources are not randomly distributed (Pilkington and Todoeschuck, 1990; Maus and Dimri, 1994; Bansal et al., 2010) which introduces some slope to the spectral decay rather than becoming white noise, implying that the slope of $\ln\langle|\Delta g(k)|^2\rangle$ vs $|k|$ gives an over estimation of the depth. Nevertheless, the depth estimates from the radially averaged power spectrum provides a good starting model for 2D and 3D interpretations.

4. Qualitative analysis and interpretation

Free-air gravity anomaly map of the study region (Fig. 2) generated using satellite derived free-air gravity data (Sandwell and Smith, 2009; Sandwell et al., 2014) generally mimic the seafloor configuration and exhibits subdued positive gravity anomalies, ranging from approximately 0 to 70 mGal along the Maldive Ridge and parts of the Deep Sea Channel between the Maldive Ridge and Chagos Bank. The Maldive Ridge segment appears to be surrounded by a broader −50 mGal contour and shows an axial low of up to −20 mGal with a width of 40 km between the latitude 2.5°N to 5.6°N along the 73.2°E meridian. Several short wavelength circular and elliptical anomalies are observed in Deep Sea Channel region. The elongated gravity highs and lows

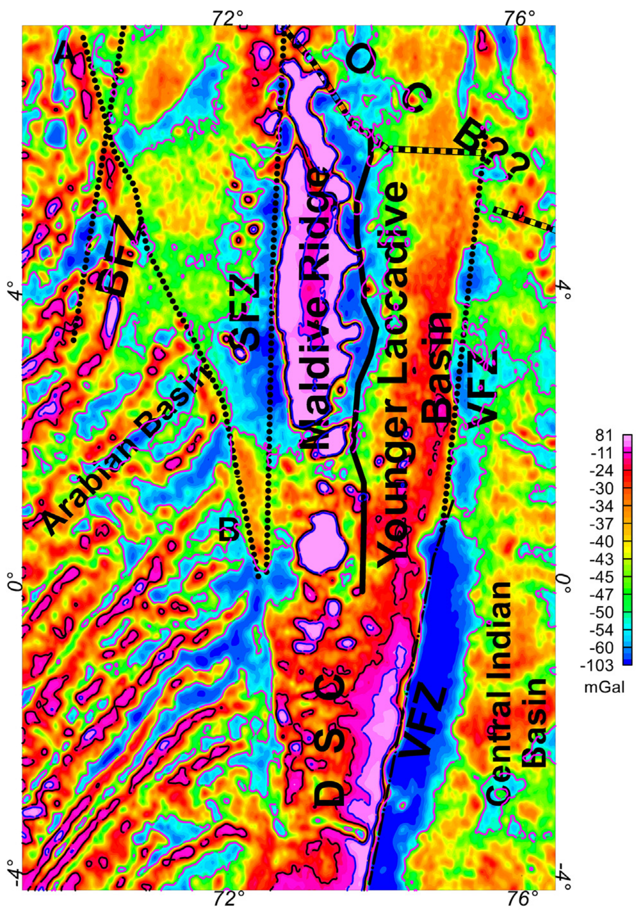

Fig. 2. High resolution satellite derived free-air gravity (FAG) anomaly map of Maldive Ridge and Adjoining areas. Crustal architecture inferred from the FAG and its transformations of the west coast of India (Kalra et al., 2014) is superposed. **VFZ**: Vishnu Fracture Zone, **SFZ**: Shiva Fracture Zone, **BFZ**: Brahma Fracture Zone, **DSC**: Deep Sea Channel, **OCB**: Ocean Continent Boundary. −50 mgal (magenta), −20 mGal (black) and 0 mGal (blue) contours are superposed. (For interpretation of the references to colour in this figure legend, the reader is referred to the web version of this article.)

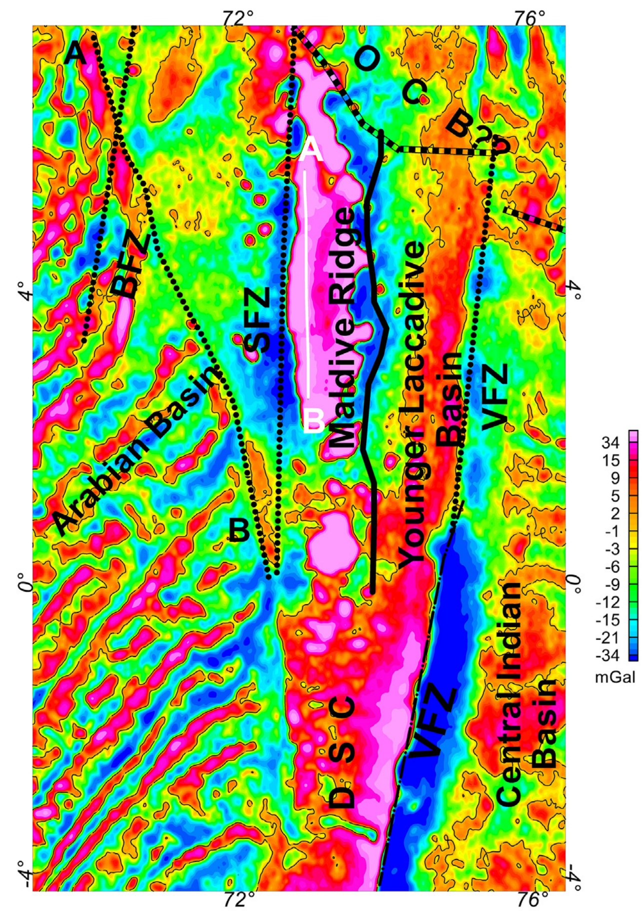

Fig. 3. Geoid corrected satellite derived free-air gravity anomaly map of the study region. The long wavelength gravity effect of Indian Ocean Geoidal Low (IOGL) is calculated using the spherical harmonic coefficient of EIGEN-6C4 (Förste et al., 2015) up to degree and order 50 and is removed from the FAG anomaly (V.24.1, Sandwell and Smith, 2009; Sandwell et al., 2014). **VFZ**: Vishnu Fracture Zone, **SFZ**: Shiva Fracture Zone, **BFZ**: Brahma Fracture Zone, **DSC**: Deep Sea Channel, **OCB**: Ocean Continent Boundary. 0 mGal contours are superposed. White line AB shows the location of the profile used for 2D forward modelling.

associated with the seafloor fabrics of the seismically active Central Indian Ridge are clearly visible on the western side of the Maldive Ridge, however towards the eastern side, in the Central Indian Basin, the signature of the seafloor fabrics appears to be imperceptible on the FAG Map. Towards the northwest, the NE-SW trending anomalies associated with the fracture zones of Central Indian Ridge is found to be terminated along the dotted line A-B. Further, the map shows a vague impression of west to eastward crossing of fracture zones over the Deep Sea Channel between 2°S and 4°S latitude with an abrupt truncation at Vishnu Fracture Zone (VFZ). Even though the north-south trending strong negative gravity anomaly of approximately −70 mGal linked with the VFZ appears to be terminated around 1°N latitude, its continuity can be traced (in patches) north of 1° but with subdued amplitudes. To have a better picture of the gravity signatures of different tectonic elements of the region, the crustal architecture of the west coast of India inferred from FAG and its transformation by Kalra et al. (2014) which falls on the northern part of the present study region is superposed in Figs. 2–4. The N-S trending gravity highs are associated with the Maldive Ridge while subdued anomalies are observed over the Younger Laccadive Basin, the region between Maldive Ridge and the Vishnu Fracture Zone.

The free-air gravity anomaly, corrected for the long wave length gravity effect of Indian Ocean Geoid Low (IOGL) (Fig. 3) depicts almost the same trend of anomalies as seen from the FAG map (Fig. 2) but with a mean increase in the amplitude of 37 mGal. The Maldive Ridge and the Deep Sea Channel clearly stands out as a north-south trending positive gravity feature along with few isolated positive highs. On either side of the ridge, the number of zero level gravity contours has substantially increased after removing the gravity effect of IOGL, signifying the state of isostatic compensation of seafloor fabrics adjacent to the ridge, previously masked by the effect of Indian Ocean Geoidal Low. However, the appearance of Maldive Ridge as a positive gravity feature over a long wavelength gravity anomaly still persists in the FAG-IOGL map. To enhance the shallow level features in the FAG-IOGL map a first vertical derivative map (FVD-FAG-IOGL, Fig. 4a) and analytic signal map (AS-FAG-IOGL, Fig. 4b) was computed (Blakely, 1995). A high pass filtered map with a cut-off wavelength of 50 km showed similar anomalies as seen in the first vertical derivative map. In both, FVD-FAG-IOGL and AS-FAG-IOGL maps (Fig. 4), the anomalies related to the fracture zones of the Arabian Basin, the northward extension of the Vishnu Fracture Zone and the highs associated with the edges of the coral reefs can be clearly demarcated which suggest that these features are observed at relatively shallow levels. The fracture zones associated with the spreading of the Central Indian Ridge within the Arabian Basin is found to be terminated at the dotted line AB. Between line AB and the

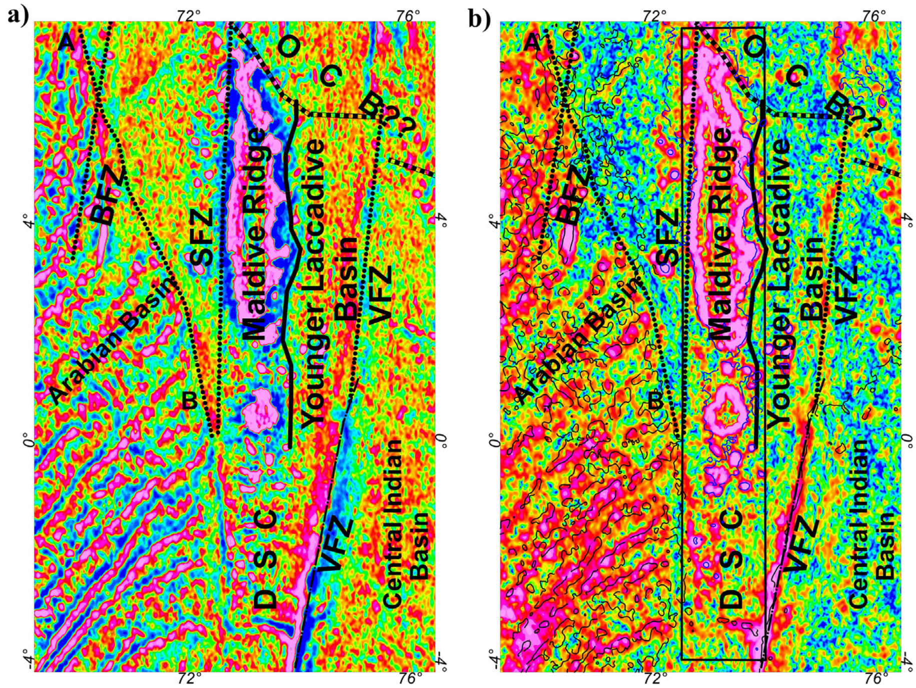

Fig. 4. (a) First Vertical Derivative (enhancing shallow features) of Indian Ocean Geoidal Low corrected Free Air Gravity (FAG-IOGL) data (b) Analytic signal map of FAG-IOGL showing the distribution of shallow level gravity anomaly sources. Bathymetric contours (4000 m-black, 2000 m-blue) are superposed. **VFZ**: Vishnu Fracture Zone, **SFZ**: Shiva Fracture Zone, **BFZ**: Brahma Fracture Zone, **DSC**: Deep Sea Channel, **OCB**: Ocean Continent Boundary. (For interpretation of the references to colour in this figure legend, the reader is referred to the web version of this article.)

Maldive Ridge, the anomalies related to fracture zone is absent implying that these are either not present in this region or is masked by the overlying strata due to which it is not traceable, each of which has its own significance on the evolution of this part of the Arabian Basin. Towards the south (south of 0°), the fracture zones are found extending eastward from the Arabian Basin into the Deep Sea Channel which are terminated further east by the Vishnu Fracture Zone. No detectable change in anomalies is observed across the OCB (delineated by Kalra et al., 2014) and within the northern part of the Central Indian Basin in the map enhancing shallow level features (Fig. 4a and b). Within the Maldive Ridge, two north-south trending relative gravity highs flank the west and the east. Seismic reflection studies (Aubert and Droxler, 1996) suggest that these highs are reef platforms. The sedimentary basin within the Maldive Ridge (Maldive Inner Sea) averaging 40 km in width, bounded by the coral reef platforms, depicts itself as relative gravity lows. Recent drilling (Betzler et al., 2017) has shown that the depositions within the Maldive Inner Sea are composed of Eocene and Oligocene neritic carbonates deposited over a volcanic basement dated at ~57 Ma (Backman et al., 1988).

To have a better understanding of the setting of the ridge, a detailed study of the Maldive Ridge and Deep Sea Channel area was undertaken. The location of the selected MR and DSC segment is shown in Fig. 4b with a rectangle. The FAG_IOGL map over the MR shows that the reef platforms, depicting as relative gravity highs, are discontinuous. The Maldive Inner Sea area is observed as a gravity low bounded by the coral reef platform. The mapped atolls (Aubert and Droxler, 1996) are superposed on Fig. 5a for comparison. The western and eastern edges of the reef platform as obtained from the analytic signal peak (AS_FAG_IOGL, Fig. 5a) clearly fall on the edges of the mapped atolls. It can also be seen that the analytic signal highs are located on the extreme western and eastern boundary of the reef platform. This suggests that the extreme western and eastern edges or the oceanward margins are generally steeply inclined while the inner boundaries are more gradational which is in accordance with the E-W cross-section across the Maldive Ridge (Betzler et al., 2017) depicting the carbonate platform stratigraphy.

As the FAG-IOGL map (Fig. 3) is composed of a mixture of short to long wavelength anomalies probably arising from sources at different depth levels, wavelength filtering operation has been carried out to separate different wavelength components. The results obtained from applying a Butterworth high pass filter with a cut-off wavelength of 50 km and low pass filter with a cut off wavelength of 100 km, over MR and DSC area is shown in Fig. 5b and c respectively. While the high pass filtered map shows the N-S trending highs associated with the oceanward margins of the atolls, the image is completely different in the low pass filtered map. It shows a relative N-S trending high along the axis of the Maldive Ridge and the Deep Sea Channel. The high associated with the edges of the atoll is not present in the 100 km low pass filtered anomaly map which suggests that the atolls are at shallow levels.

To determine the depth to the top of the different density interfaces over the Maldive Ridge and Deep Sea Channel (DCS), the power spectral method (Spector and Grant, 1970; Mishra, 2011) was utilized. For arriving at an optimum window length for power spectral analysis, we have selected the locations of the broadband seismic stations on the Maldive Ridge (KAAM and HMDM) where depth to different interfaces were available for comparison with the results obtained from the power spectrum. We started with a window dimension of 50 km by 50 km, calculated the depths using power spectral analysis and compared with the depths from broadband seismic stations. This process was repeated by increasing the dimensions by 10 km. A good comparison was obtained for window dimensions of 110 km by 110 km. This window length was then tried in the Deep Sea Channel area where two seismic refraction stations were available which also gave comparable results. Hence the entire region was divided into several blocks with each block having a dimension of 110 km by 110 km. With a 50% overlap between the adjacent blocks, we have 44 blocks covering the Maldive Ridge and DSC. The computed radially-averaged power spectrum can be divided into several straight line segments, the slope of each segment giving the average depth to the top of the corresponding interfaces (Spector and Grant, 1970; Blakely, 1995) with detectable density contrast. Radially averaged power spectrum of a few representative blocks are shown in Fig. 6. In the present study, the slopes of the line segments were accepted only if the coefficient of determination of the fit is greater than 0.96, otherwise discarded. For each block two straight line segments were obtained; the higher frequency segment represents the average depth to the top of the shallow interface and the lower frequency segment represents the ensemble average depth to the top of the deeper layer. The uncertainty in the estimated depths, which arises due to the

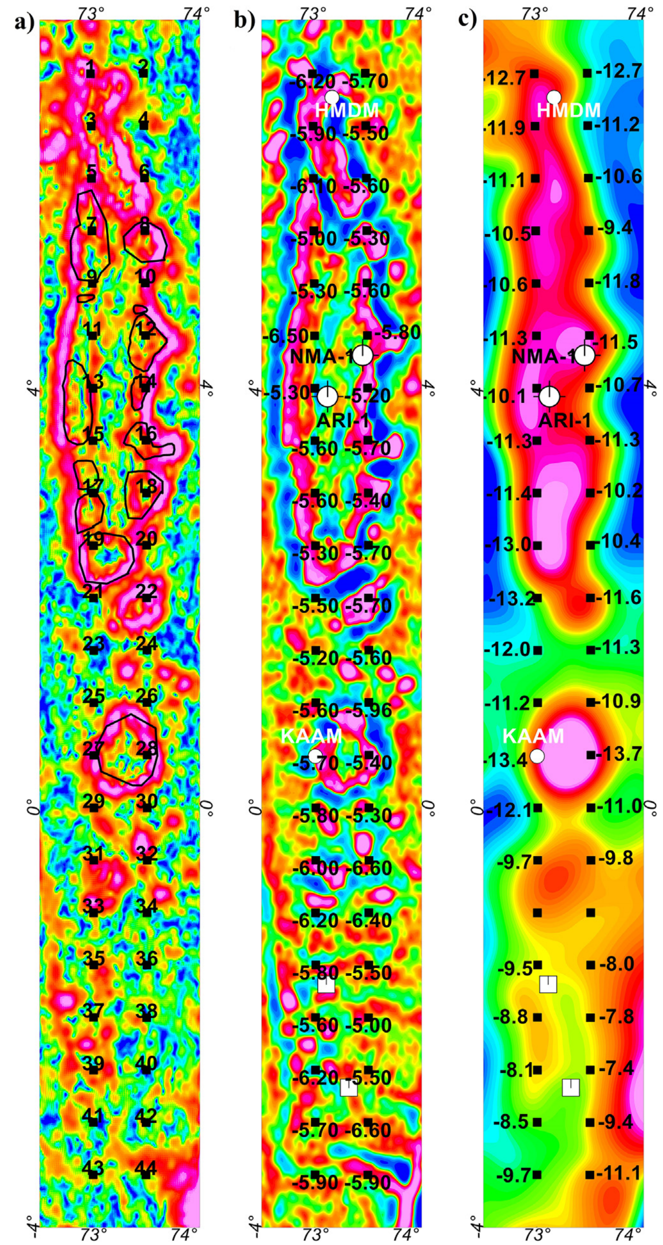

Fig. 5. (a) Analytic signal map over the Maldive Ridge and Deep Sea Channel showing the distribution of gravity anomaly sources at shallow depths. Closed lines show the location of atolls. Filled box with numbers shows the location of centre point and segment numbers of the windows used for the calculation of radially averaged power spectrum (b) High pass filtered map of FAG-IOGL data with a cut-off wavelength of 50 km. Superposed are the depth to the top of the shallow layer (segment-2) obtained from radially averaged power spectrum (z is taken positive up). ARI-1 and NMA-I shows location of industrial wells (Aubert and Droxler, 1996), KAAM and HMDM location of broadband seismic stations (Fontaine et al., 2015) and white box represents location of seismic refraction stations (Francis and Shor, 1966) (c) Low pass filtered map of FAG-IOGL data with a cut-off wavelength of 100 km. Superposed are depths to top of the deeper layer (segment-1) computed using radially averaged power spectrum.

various assumptions made in the computation of the radially averaged power spectrum, will be of the order of 10–15% (Mishra and Pedersen, 1982). The centre of each block is shown in Fig. 5a. The average depth to the top of the deeper segment (segment-1) along the western side of the ridge is 11 km while that of the eastern side is 10.8 km. The average depth to the top of the shallow layer (segment-2) over the ridge is 5.5 km. The depths calculated using the power spectral methods will be on the higher side, especially the computed depths of the shallow segment, as the window length of 110 km used for the computations will include a contribution from adjoining areas of the ridge as well in addition to the assumption of random uncorrelated sources.

5. Discussion

To compare the results obtained from the qualitative and power spectral analysis and to demarcate the lithology giving rise to the density contrast across the mapped interface, the results from the three seismic refraction stations (station 1, 4, and 5 of Francis and Shor, 1966), the drilled wells (Backman et al., 1988; Duncan and Hargraves, 1990; Aubert and Droxler, 1996) and the two broadband seismometers (Fontaine et al., 2015), located along the Chagos-Maldive-Laccadive Ridge axis (see Fig. 1 for location), were utilized. In the northernmost refraction station, located slightly north of the study area, between the Laccadive and Maldive islands, a 3 km-thick volcanic layer, with a P-wave velocity of 5.0 km/s was delineated overlying a 10 km-thick oceanic crustal layer with an average velocity of 6.84 km/s. Along the second station, located in the Deep Sea Channel separating the Maldives and Chagos, a 4–5 km-thick layer, characterized by an average velocity of 6.13 km/s, overlies a 7.1 km/s crustal layer. Three ODP drilling sites (714, 715 and 716) are located in the northern part of the Maldive Ridge. Drilling at Site 715, located in water depths of about 2262 m, reached the basaltic basement (lava flows) at about 211 m below seafloor. NMA-1(Elf) well, drilled over an atoll, terminated at 2222 m after drilling through 116 m thick basal unit composed of weathered basaltic flows. ARI-1 well drilled in the Maldive Inner Sea penetrated a 50 m thick basal unit composed of weathered basaltic flows at a depth of 3365 m. The top of the basaltic flow is at an approximate depth of 2051 m, 2106 m and 3315 m from sea level respectively at ODP 715, NMA-1 and ARI-1 well locations. Dating of the basaltic samples from wells ODP 715 and NMA-1 using $^{40}Ar/^{39}Ar$, yielded ages of 57.2 Ma and 55 Ma, respectively (Aubert and Droxler, 1996). Seismic reflection studies over the Maldive Ridge and the Maldive Inner Seas, suggests that the carbonate platform is underlain by volcanic basement which is sub-divided into a layer of lava flow unit (penetrated through drilling), followed by an acoustic basement whose surface is highly discontinuous due to sub-vertical faulting (Aubert and Droxler, 1996; Betzler et al., 2017). By utilizing the velocities of cored basalts from site ODP 715 (Backman et al., 1988) and the travel time values (Aubert and Droxler, 1996) obtained from seismic reflection studies, it can be assumed that the sub-areal lava flows in the Maldive Ridge area will have a thickness of approximately 1–1.5 km. Also, interpretation of a large grid of seismic reflection profiles suggests that the Eocene carbonate banks were established on topographic highs of the faulted volcanic basement (Belopolsky and Droxler, 2003). From the N-S and E-W transects across the Maldives platform (Aubert and Droxler, 1996; Belopolsky and Droxler, 2003) constructed from integrating seismic reflection and well information, it can be inferred that the top of the volcanic layer (lava flow unit) is at an average depth of 2.5–3 km over the atolls and 3.5–4 km in the Maldive Inner Sea (MIS) area. So the approximate depth to the top of the acoustic basement unit will be of the order of 3.5–4.5 km over the atolls and 5–5.5 km in the MIS region. Receiver function analysis of the broadband seismic stations located over the Maldive Ridge (HMDM and KAAM) showed a seismic discontinuity (Fontaine et al., 2015) around 4 km which may probably be representing the top of the acoustic basement and thus support the present inference. The spectral analysis gave an average depth of 5.5 km as depth to the top of the shallow interface (segment-2). Comparing this with the result from seismic data and well information discussed above, it can be inferred that this depth may correspond to depth to the top of the acoustic basement. To compare the deeper interface (segment-1) which is at an average depth of 11.0 km over the MR, the depth estimates from the broadband seismic stations at HMDM and KAAM were

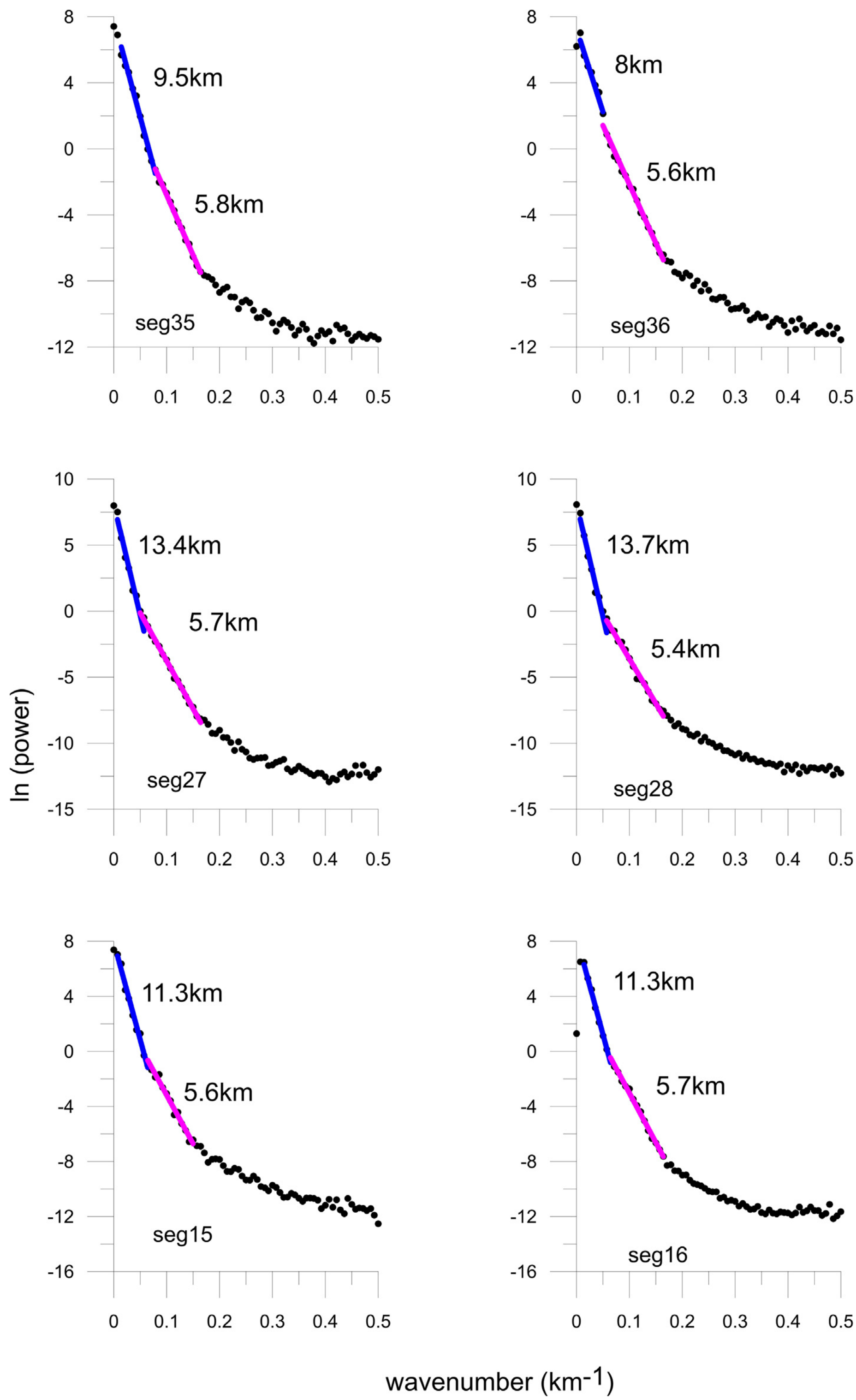

Fig. 6. Radially averaged power spectrum of a few representative blocks. Fig. 5 for segment location.

utilized. At both these stations, the V_s velocity is between 4.4 and 4.6 km/s at an average depth of 13.5 km, which was interpreted as representing the initial Moho depth, i.e., before the formation of magmatic underplated rocks (Fontaine et al., 2015). At KAAM the depth obtained from receiver function analysis of the broadband seismic stations is 13 km while that obtained from the present study is 13.5 km. At station HMDM, the Moho depth obtained is 14 km while that obtained from free-air gravity data is 12.1 km which is the average value from 4 stations surrounding HMDM. This difference is within the error limit of depths calculated using the power spectral methods. Thus the average depth of 11 km, obtained from power spectral methods, can be inferred as the initial Moho depth before the formation of the underplated rocks.

To compare the depth estimated using radially averaged power spectrum, we have undertaken a 2-dimensional forward modelling of the FAG_IOGL data along a N-S profile roughly coinciding with a part of the western side of the Maldive Ridge (profile location is shown in Fig. 3). This part of the western segment was chosen as we had seismic constraints (Aubert and Droxler, 1996) to start the gravity modelling. A similar exercise was not undertaken in the Deep Sea Channel region as there were no other data to constrain the gravity modelling. The 2D forward modelling was performed using the interactive GM-SYS Profile Modelling software (Geosoft, 2014). The modelling involves creating a crustal model using available geophysical constraints and computing the model gravity response based on the methods of Talwani et al., (1959) and makes use of the algorithms described in Won and Bevis (1987). A two-dimensional flat earth model was assumed and the USGS SAKI (Webring, 1985) implementation of the Marquardt inversion algorithm was used to linearize and invert the data. Owing to the non-uniqueness of the potential field models, the authenticity of the final geological model depends on how well the initial model is constrained. To start with, we assumed a multi-layered model with the top-most layer as bathymetry followed by carbonate reefs atop the volcanic basement (lava flow unit), constrained using the thicknesses from published N-S seismic transect (Aubert and Droxler, 1996). The layer of volcanic flow is followed by the acoustic basement, underplated materials and finally the mantle. Initially, the depth to the top of the acoustic basement and underplated materials was assumed from spectral depth estimates while Moho depth was constrained from our previous study (Kunnummal et al., 2018). The layer of the carbonates ranging in age from Paleogene to present was assumed an average density of 2.3 gm/cc while the lava flows was assigned an average density of 2.8 gm/cc (Backman et al., 1988). The acoustic basement, underplated material and Moho were respectively provided densities of 2.95 gm/cc, 3.05 gm/cc and 3.30 gm/cc. The gravity response of this model was computed and compared with the observation. The depth to the top of the different crustal layers and Moho was iteratively adjusted to minimize the error between the observed and computed response. The final crustal model with the minimum RMS error is shown in Fig. 7.

The depths to the top of the different layers were estimated from the 2D model. It can be seen from the 2D model that the lateral variation of the different interfaces is very smooth except for minor undulations over the acoustic basement which was noted previously in seismic reflections (Aubert and Droxler, 1996). The average depth to the top of the lava flow unit of the volcanic basement, underlying the atolls, is 2.6 km from MSL which matches well with the depth to the top of the basaltic flows obtained from drilled wells, as mentioned earlier. The average thickness of the acoustic basement along the modelled profile is of the order of 5.5 km. Along the profile, the Moho is at an average depth of 25 km. For comparison of the modelled depth along the western segment of MR with that of the spectral depth estimates and Moho undulations (Kunnummal et al., 2018), we have marked the depths obtained for different layers in Fig. 8. The minor differences can be attributed to the techniques and the inherent assumptions & calculation methodology used in these techniques.

Integrating results from the present study, with the available geophysical data, an attempt has been made to generate a geological cross-section along two north-south profiles using the depth values of different segments along the west and east blocks (Fig. 8). In this cross-section, the region between, segment-1 (deeper layer i.e., top of underplated material) and segment-2 (shallow layer i.e., top of acoustic basement) is called as “crust” since we have not distinguished it as either oceanic or continental or volcanic even though the 2D forward model has provided better estimates assuming a density of 2.95 gm/cc which is close to oceanic crustal density. Also, we have not obtained any density interfaces within the “crust”. It is worth mentioning here that the shear wave velocity at stations KAAM and HMDM show velocity discontinuities at approximately 10 km and 8 km respectively. Depth to the top of the present Moho computed from the inversion of Mantle Residual Gravity Anomalies after applying necessary corrections for sediments and lithospheric pressure and temperature anomalies (Kunnummal et al., 2018) is also utilized in the geological cross-section.

It can be seen from the generated geological cross-section (Fig. 8) that there is a marked change in the depth to the top of the underplated

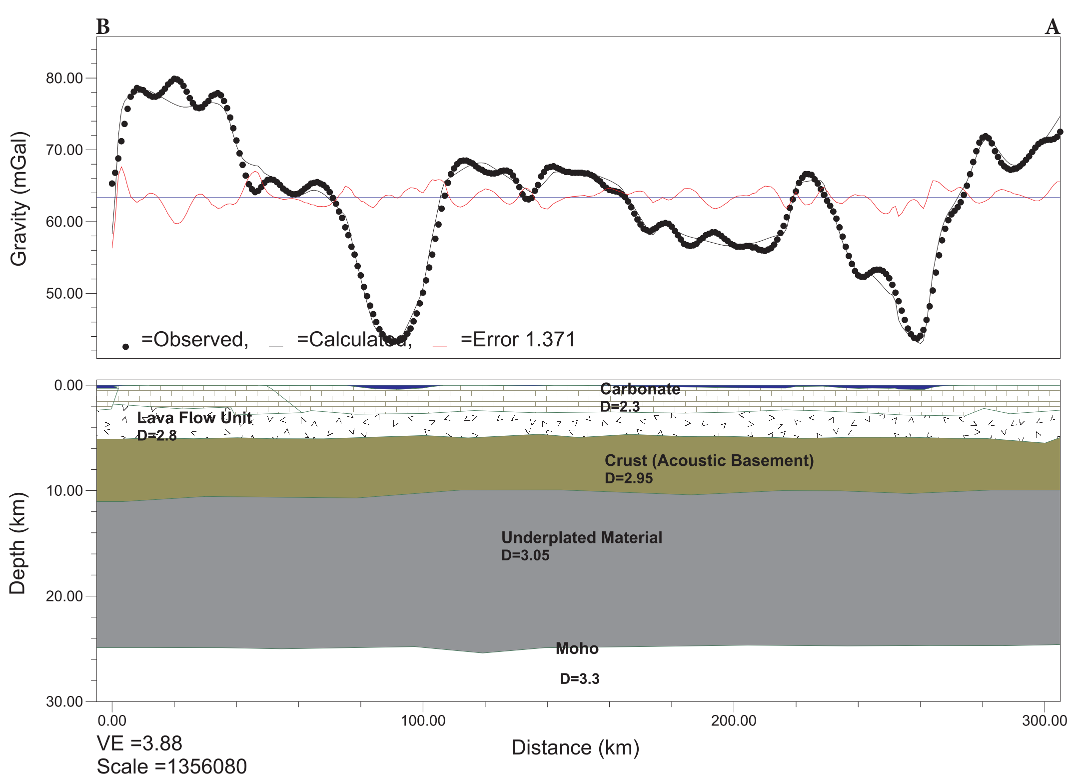

Fig. 7. Two dimensional crustal model derived from the FAG-IOGL gravity data analysis along a N-S profile over the Maldive Ridge; location of the profiles is given in Fig. 3. The water depths, thickness of carbonate sediments and depth to top of lava flows have been obtained from seismic sections (Aubert and Droxler, 1996). Dotted lines represent the observed while the full lines depict the calculated values and the thin red lines depict the errors. (For interpretation of the references to colour in this figure legend, the reader is referred to the web version of this article.)

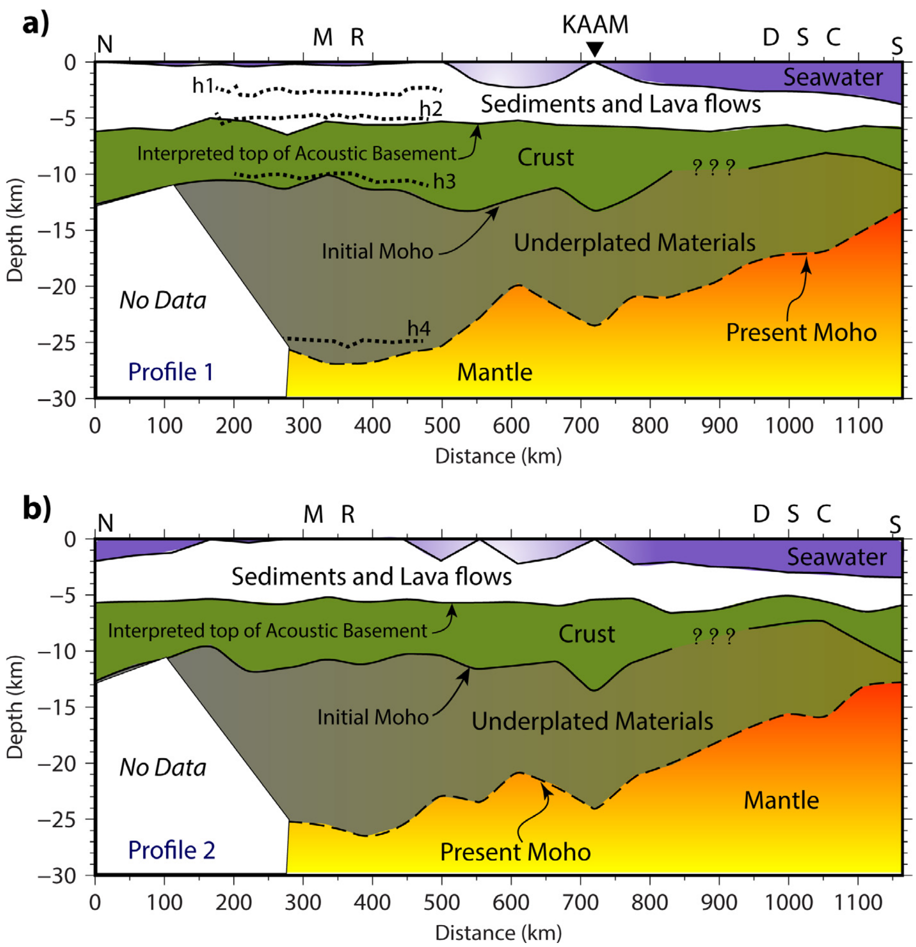

Fig. 8. Sketch showing a possible geological cross-section along two N-S profiles across the Maldive Ridge and the Deep Sea Channel. Bathymetry from Smith and Sandwell (1997). Depth to top of "Interpreted Acoustic Basement" from segment 2 of power spectrum and depth to top of "Initial Moho" from segment 1 of the power spectrum. Layers interpreted by integrating with available data, as discussed in the text. No data control over sediments and lava flows. Depth to top of present Moho is from the inversion of Mantle Residual Gravity Anomalies (Kunnummal et al., 2018). Profile-1 (western) generated using depths from segments (1, 3, 5,… 43) and Profile-2 (eastern) from segments (2, 4, 6, …, 44). Locations of segments in Fig. 5. Dotted lines h1, h2, h3, h4 respectively represent depth to top of subaerial lava flows, acoustic basement, underplated material and Moho computed from 2D forward model (Fig. 7).

material north and south of 0° i.e., the "crust" is relatively thin in the Deep Sea Channel region. The average depth to the initial Moho (bottom of "crust"/top of underplated material) north of 0° is 11.5 km while that to the south is 8.8 km (two extreme values are not considered for averaging). The average depth to the top of a 7.11 km/s velocity layer inferred from seismic refraction stations (location is shown in Figs. 1 and 5b) in the Deep Sea Channel (region south of 0°) is 8.3 km, thus matching with the depths computed from gravity data. This shows the depth to top of the underplated material (representing the initial Moho) is at a shallower level along the DSC. The average water depth and sediment thickness in the DSC area are 3.0 km and 1 km respectively which when subtracted from the depth to top of underplated material (i.e., ~8.8 km) gives a thickness of ~4.8 km (thickness of "crust"/acoustic basement) which roughly coincides with the crustal thickness estimated from the two seismic refraction stations (3.9 km at station 4 & 4.9 km at station 5). The layer with a velocity of 6.13 km/s, which may be considered as oceanic crustal velocity, is estimated to have an average thickness of approximately 4.4 km (Francis and Shor, 1966). In this region, from the present study, the extension of fracture zones has been delineated that are associated with the Central Indian Ridge spreading centre as high-frequency gravity anomaly (from the first vertical derivative map, Fig. 4a). Avraham and Bunce (1977) identified large magnetic anomalies along a N-S profile in this region. They also argued that the DSC region may be a part of a transform fault along which India was moving to the north. Through simulation of three-dimensional numerical models, Bredow et al. (2017) showed that in the DSC region, the Reunion plume was above a long transform fault that disrupted the melt generation. This suggests in the present model as a marked decrease in the thickness of underplated material in the Deep Sea Channel compared to the Maldive Ridge segment. Also, the interaction with long transform fault might have hindered the subaerial lava flows (above the acoustic basement) in this region due to which the fracture zones associated with spreading of Central Indian Ridge is not masked and was detectable in the first vertical derivative map. Crustal thickness of ~4.8 km along with the presence of fracture zones and velocity of 6.13 km/s may be suggestive of an oceanic crust underlying the Deep Sea Channel region.

The depth to the top of the acoustic basement by and large is flat along the axis of the Maldive Ridge as well as the Deep Sea Channel, suggesting that this is a continuous structure. The flatness of this interface provides evidence about the Maldivian physiography that this was more of an elongated plateau forming the basement for later deposition rather than a ridge with significant topographic relief like the Ninety East Ridge. The relief of the acoustic basement with respect to the adjoining Arabian Basin and the Central Indian Basin is not considered here. However, the deeper layer, interpreted as depth to top of the magmatic underplating, is thicker underneath the Maldive Ridge, thinner over the DSC and again thickens further south of DSC towards the Chagos Bank. Moho undulations mapped by inverting the Mantle Residual Gravity Anomalies (Kunnummal et al., 2018) after applying sediment and lithospheric pressure-temperature corrections show a similar pattern with deeper Moho beneath the Maldive Ridge and thinning over the Deep Sea Channel region. Even though the depth to the top of acoustic basement (inferred to represent oceanic crust in the DSC region) is continuous along the MR and DSC, we are unable to find any anomalies related to fracture zones along the Maldive Ridge, hence the nature of the crust underlying MR cannot be inferred. Also, it has been previously reported that no seafloor spreading magnetic anomalies are identified on top and along the Maldive Ridge (Avraham and Bunce, 1977). One of the possible reasons suggested for the non-identification of spreading anomalies being the masking of these anomalies by the overlying lava flows. In the Laccadive part of the CLR, several short wavelength gravity anomalies were interpreted as the expression of the intrusives along the pre-existing faults as the Indian plate moved over the Reunion hotspot (Nair et al., 2013). Similar high-frequency anomalies are not observed over the Maldive Ridge. From receiver function analysis of broadband seismic network over Chagos Bank, a change in velocity was observed at a depth of 12 km interpreted as the initial Moho depth (Fontaine et al., 2015) which matches with the average depth of 11.5 km obtained over the MR showing a similarity of initial Moho depth between these two ridges. Even though the MR shows similarity as well as dissimilarity with Chagos Bank and Laccadive Ridge, both of which are earlier interpreted as underlain by continental crust (Chaubey et al., 2002; Torsvik et al., 2013; Nair et al., 2013), at this juncture it is not possible to conclusively comment on the nature of the MR i.e., whether it is oceanic or continental in origin. Additional geophysical information as well as geochemical data from deep sea drilling at different locations over the MR will go a long way in deciphering the nature of the Maldive Ridge segment of the Chagos Laccadive Ridge.

6. Conclusions

High resolution satellite derived free-air gravity (FAG) anomalies over the Maldive Ridge (MR), Deep Sea Channel (DSC) between Maldive Ridge and Chagos Bank and parts of the adjoining Arabian Basin and Central Indian Basin was analysed to have a qualitative understanding on the structural set up of the Maldive Ridge and DSC. Various transformation operations including wavelength filtering were carried out on the Indian Ocean Geoidal Low (FAG-IOGL) corrected free-air gravity data to isolate the gravity sources at different depth levels. From the analysis, we found that Vishnu Fracture Zone extends north of 0°N and extend into the previously assumed ocean continent boundary (Kalra et al., 2014). While the gravity anomalies associated with the shallow to intermediate wavelength anomalies over the MR reflects the reef platforms/top of the lava flow unit/acoustic basement, the long wavelength anomalies reflect the signature of the underplated material related to the movement of Indian plate over the Reunion hotspot. Depth to top of shallow and deep interfaces over the MR and DSC were computed from the radially averaged power spectrum of the FAG-IOGL gravity data for a window of 110 km by 110 km. The shallow interface gave an average depth of 5.5 km from the surface while the deeper interface was found to lie at an average depth of 11.0 km. The depths obtained from spectral analysis were compared to that computed from two-dimensional forward modelling along a N-S profile along the western segment of the Maldive Ridge. Integrating the results obtained from the present study with available seismic refraction, reflection, drilled wells, broad band seismic data supported by the 2D forward model, it was inferred that the shallow depth corresponds to the top of the acoustic basement (Aubert and Droxler, 1996) and the deeper reflects the depth to the top of the initial Moho before the formation of magmatic underplated rocks. The Deep Sea Channel is interpreted to be purely oceanic in nature with the delineation of the extension of fracture zones in this region. To comment on the nature of the Maldive Ridge segment of the CLR, further studies including combined modelling and inversion of potential field (gravity and magnetic) anomalies has to be undertaken. In addition, information from geophysical surveys including magnetic data along with geochemical data from deep drilling at several locations on the ridge will prove useful in deciphering the nature of the ridge.

Acknowledgement

We thank the Director of the Indian Institute of Geomagnetism, Mumbai, for his constant encouragement and support and according permission to publish this work. Funds for carrying out this research at the Indian Institute of Geomagnetism is provided by the Department of Science and Technology (DST), Government of India, New Delhi. We gratefully acknowledge the Editor, and review by an anonymous reviewer on an earlier version of the manuscript that has helped improve the paper. We also thank Dr. Meghan S Miller, Associate Professor, The Australian National University and Dr. Nisha Nair, Scientist NCAOR, for their comments, suggestions and editing support on an earlier version of this MS. Figs. 1 and 8 are generated using GMT Software (Wessel and Luis, 2017).

References

Ajay, K.K., Chaubey, A.K., Krishna, K.S., Gopala Rao, D., Sar, D., 2010. Seaward dipping reflectors along the SW continental margin of India: Evidence for volcanic passive margin. J. Earth Syst. Sci. 119, 803–813.

Ashwal, L.D., Wiedenbeck, M., Torsvik, T.H., 2017. Archaean zircons in Miocene oceanic hotspot rocks establish ancient continental crust beneath Mauritius. Nat. Commun. 8, 1–9.

Aubert, O., Droxler, A.W., 1996. Seismic stratigraphy and depositional signatures of the Maldive carbonate system (Indian Ocean). Mar. Petrol. Geol. 13, 503–536.

Avraham, B.Z., Bunce, E.T., 1977. Geophysical study of the Chagos-Laccadive Ridge, Indian Ocean. J. Geophys. Res. 82, 1295–1305.

Backman, J., Duncan, R.A., et al., 1988. Proc. ODP, Init. Repts., 115: College Station, TX (Ocean Drilling Program), pp. 589–656.

Bansal, A.R., Gabriel, G., Dimri, V.P., 2010. Power law distribution of susceptibility and density and its relation to seismic properties: an example from the German Continental Deep Drilling Program. J. Appl. Geophys. 72, 123–128.

Belopolsky, A., Droxler, A., 2003. Imaging tertiary carbonate system. The Maldives. Indian Ocean. Lead. Edge 22, 646–652.

Belopolsky, A.V., Droxler, A.W., 2004. Seismic expressions and interpretation of carbonate sequences: the Maldives platform, equatorial Indian Ocean. AAPG Stud. Geol. 49, 1–46.

Betzler, C., Eberli, G.P., Alvarez Zarikian, C.A., Alonso-García, M., Bialik, O.M., Blättler, C.L., Guo, J.A., Haffen, S., Horozal, S., Inoue, M., Jovane, L., Kroon, D., Lanci, L., Laya, J.C., Ling Hui Mee, A., Lüdmann, T., Nakakuni, M., Nath, B.N., Niino, K., Petruny, L.M., Pratiwi, S.D., Reijmer, J.J.G., Reolid, J., Slagle, A.L., Sloss, C.R., Su, X., Swart, P.K., Wright, J.D., Yao, Z., and Young, J.R., 2017. Expedition 359 summary. In Betzler, C., Eberli, G.P., Alvarez Zarikian, C.A., and the Expedition 359 Scientists, Maldives Monsoon and Sea Level. Proceedings of the International Ocean Discovery Program, 359: College Station, TX (International Ocean Discovery Program).

Bhattacharya, G.C., Chaubey, A.K., 2001. Western Indian Ocean – a glimpse of the tectonic scenario. In: Sen Gupta, R., Desa, E. (Eds.), The Indian Ocean – A perspective. Oxford-IBH, New Delhi, pp. 691–729.

Blakely, R.J., 1995. Potential Theory in Gravity and Magnetic Applications. Cambridge University Press.

Bredow, E., Steinberger, B., Gassmöller, R., Dannberg, J., 2017. How plume-ridge interaction shapes the crustal thickness pattern of the Réunion hotspot track. Geochem. Geophys. Geosyst. 18, 2930–2948.

Cande, S.C., Patriat, P., 2015. The anticorrelated velocities of Africa and India in the Late Cretaceous and early Cenozoic. Geophys. J. Int. 200, 227–243.

Chaubey, A.K., Gopala Rao, D., Srinivas, K., Ramprasad, T., Ramana, M.V., Subrahmanyam, V., 2002. Analyses of multichannel seismic reflection, gravity and magnetic data along a regional profile across the central-western continental margin of India. Mar. Geol. 182, 303–323.

Chaubey, A.K., Srinivas, K., Ashalatha, B., Rao, D.G., 2008. Isostatic response of the Laccadive Ridge from admittance analysis of gravity and bathymetry data. J. Geodyn. 46, 10–20.

Duncan, R.A., Hargraves, R.B., 1990. In: Duncan, R.A., Backman, J., Peterson, L.C., et al., (Eds.), Proceedings of the Ocean Drilling Program, College Station, Texas, Scientific Results 115, pp. 43–51.

Fontaine, F.R., Barruol, G., Tkalčić, H., Wölbern, I., Rümpker, G., Bodin, T., Haugmard, M., 2015. Crustal and uppermost mantle structure variation beneath La Réunion hotspot track. Geophys. J. Int. 203, 107–126.

Förste, C., Bruinsma, S., Abrikosov, O., Lemoine, J, M., Marty, J, C., Flechtner, F., Balmino, G., Barthelmes, F., Biancale, R., 2015. EIGEN-6C4, The latest combined global gravity field model including GOCE data up to degree and order 2190 of GFZ Potsdam and GRGS Toulouse. GFZ Data Services.

Francis, T.J.G., Shor, G.G., 1966. Seismic refraction measurements in the northwest Indian Ocean. J. Geophys. Res. 71, 427–449.

Geosoft, 2014. Oasis montage data processing and analysis (DPA) systems for Earth Science Applications (ver.8.0), GM-SYS version 7.0 Gravity and magnetic modeling software user guide Geosoft Inc, Canada.

Kahle, H.G., Chapman, M., Talwani, M., 1978. Detailed 1×1 gravimetric Indian Ocean Geoid and comparison with Geos-3 radar altimeter geoid profiles. Geophys. J. R. Astron. Soc. 55, 703–720.

Kalra, R., Srinivasa Rao, G., Fainstein, R., Radhakrishna, M., Bastia, R., Chandrashekar, S., 2014. Crustal architecture and tectono-magmatic history of the western offshore of India: Implications on deepwater sub-basalt hydrocarbon exploration. J. Pet. Sci. Eng. 122, 149–158.

Karner, G.D., 1982. Spectral representation of isostatic models. BMR J. Aust. Geol. Geophys. 7, 55–62.

Kunnummal, P., Anand, S.P., Haritha, C., Rama Rao, P., 2018. Moho depth variations

over the Maldive Ridge and adjoining Arabian and Central Indian Basins, Western Indian Ocean, from three dimensional inversion of gravity anomalies. J. Asian Earth Sci. 156, 316–330.
Majumdar, T.J., Mohanty, K.K., Srivastava, A.K., 1998. On the utilization of ers-1 altimeter data for offshore oil exploration. Int. J. Remote Sens. 19, 1953–1968.
Maus, S., Dimri, V.P., 1994. Scaling properties of potential fields due to scaling sources. Geophys. Res. Lett. 21, 891–894.
McKenzie, D., Sclater, J.G., 1971. The evolution of the Indian Ocean since the late cretaceous. Geophys. J. R. Astron. Soc. 25, 437–528.
Mishra, D.C., 2011. Gravity and magnetic methods in geological studies: Principles, integrated exploration and plate tectonics. B.S. Publications, Hyderabad, ISBN: 978-93-81075-27-2.
Mishra, D.C., Pedersen, L.B., 1982. Statistical analysis of potential fields from surface relief. Geo-exploration 19, 247–265.
Müller, R.D., Sdrolias, M., Gaina, C., Roest, W.R., 2008. Age, spreading rates, and spreading asymmetry of the world's ocean crust. Geochem. Geophys. Geosyst. 9, 1–19.
Nabighian, M.N., 1984. Toward a three-dimensional automatic interpretation of potential field data via generalized Hilbert transforms: Fundamental relations. Geophysics 49, 780–786.
Nair, N., Anand, S.P., Rajaram, M., 2013. Tectonic framework of Laccadive Ridge in Western Continental Margin of India. Mar. Geol. 346, 79–90.
Pilkington, M., Todoeschuck, J.P., 1990. Stochastic inversion for scaling geology. Geophys. J. Int. 102, 205–217.
Sandwell, D.T., Müller, R.D., Smith, W.H.F., Garcia, E., Francis, R., 2014. New global marine gravity model from CryoSat-2 and Jason-1 reveals buried tectonic structure. Science 346, 65–67.
Sandwell, D.T., Smith, W.H.F., 2009. Global marine gravity from retracked Geosat and ERS-1 altimetry: Ridge segmentation versus spreading rate. J. Geophys. Res. 114, B01411.
Smith, W.H., Sandwell, D., 1997. Global sea floor topography from satellite altimetry and ship depth soundings. Science 277, 1956–1962.
Spector, A., Grant, F.S., 1970. Statistical models for interpreting aeromagnetic data. Geophysics 35, 293–302.
Sreejith, K.M., Rajesh, S., Majumdar, T.J., Rao, G.S., Radhakrishna, M., Krishna, K.S., Rajawat, A.S., 2013. High-resolution residual geoid and gravity anomaly data of the northern Indian Ocean – an input to geological understanding. J. Asian Earth Sci. 62, 616–626.
Talwani, M., Worzel, J.L., Landisman, M., 1959. Rapid gravity computations for two dimensional bodies with application to the Mendocino submarine fracture zone. J. Geophys. Res. 64, 49–59.
Torsvik, T.H., Amundsen, H., Hartz, E.H., Corfu, F., Kusznir, N., Gaina, C., Doubrovine, P.V., Steinberger, B., Ashwal, L.D., Jamtveit, B., 2013. A Precambrian microcontinent in the Indian Ocean. Nat. Geosci. 6, 1–5.
Webring, M.W., 1985. SAKI: a Fortran program for generalized linear inversion of gravity and magnetic profiles. USGS Open File Report 85–122.
Wessel, P., Luis, J.F., 2017. The GMT/MATLAB Toolbox. Geochem. Geophys. Geosyst. 18.
Won, I.J., Bevis, M.G., 1987. Computing the gravitational and magnetic anomalies due to a polygon: Algorithms and FORTRAN subroutines. Geophys. 52, 232–238.